The Thesis Committee for Deyun Li
Certifies that this is the approved version of the following thesis :

An exploration on electron bunching of ionization induced self-injection in laser wakefield accelerators

APPROVED BY
SUPERVISING COMMITTEE:

Supervisor:

Gennady Shvets

Herbert Berk

An exploration on electron bunching of ionization induced self-injection in laser wakefield accelerators

by

Deyun Li, B.S.

Thesis

Presented to the Faculty of the Graduate School of

The University of Texas at Austin

in Partial Fulfillment

of the Requirements

for the Degree of

MASTER OF ARTS

The University of Texas at Austin

May 2016

Acknowledgements

This thesis could not be completed without the assistance of many scientists. Firstly, thank you to my supervisor, Professor Gennady Shvets, for taking me into his group and guiding this research. I would also like to thank Drs. Vladimir Khudik for inspiring me with this topic and helped me so much in the daily research. Furthermore, I must thank Drs. Xi Zhang and Tao Wang for the numerous help theoretically and technically all the way through this work.

Abstract

An exploration on electron bunching of ionization induced self-injection in laser wakefield accelerators

Deyun Li, M.A.

The University of Texas at Austin, 2016

Supervisor: Gennady Shvets

Plasma-based wakefield accelerator is attractive for generating quasi-monoenergetic electron beams using the bubble regime. The bubble is formed by an intense driver, which propagates through the plasma and expels all electrons transversely, creating a cavity free of cold plasma electrons that trailing behind the driver. Self-injection is applicable in the bubble regime, which can produce bunches of quasi-monoenergetic electrons. (1) Such electron bunching structure can be diagnosed with coherent transition radiation and may be exploited to generate powerful high frequency radiation [16].This thesis focuses on electron bunching phenomenon through WAKE simulations and theoretical analysis. The

simulation is completed under laser-driven field ionization wakefield acceleration. The code is improved by taking into consideration the high frequency property of laser driver in wakefield acceleration. Finer grid size is introduced to the ionization injection part of WAKE, for increasing simulation accuracy without much sacrifice of programming efficiency. Various conditions for optimal bunching in the trapped electrons are explored computationally and analytically.

Table of Contents

List of Figures viii

Chapter 1: Introduction 1

1.1 History of plasma-based accelerators 1

1.2 Driving mechanism in laser wakefield acceleration 5

1.3 Bubble regime formation and advantages 8

1.4 Self-injection schemes 12

1.4.1 Self-injection in the temporally evolving bubble 12

1.4.2 Field ionization induced self-injection 15

1.5 Summary 20

Chapter 2. Electron bunching in ionization induced self-injection 22

2.1 The high-frequency laser pulse driver and self-injected electrons 22

2.2 Parameters for laser driver and simulation domain 26

2.3 Electron trapping dynamics in the highly nonlinear bubble 27

2.4 Conditions for effective electron bunching 35

Chapter 3. Conclusion 39

References 41

List of Figures

Figure 2.1: Profile of an 800nm laser pulse's intensity 23

Figure 2.2: Electrons' injection distribution 25

Figure 2.3: Profiles for laser pulse intensities with different grid size $\Delta\xi$ 26

Figure 2.4: Phase space trajectories for electron in 1st stage.....28

Figure 2.4: Electron bunching and FFT analysis 32

Figure 2.5: Phase space distribution for one slice of injected electrons 35

Figure 2.6: Bunching factor plots for trapped electrons 37

List of Illustrations

Figure 1.1: Schemes of four basic plasma-based accelerators [19] 3

Figure 1.2: Relation of plasma density and excited electric field [22] 7

Figure 1.3: Electron density cavities (bubble region) in LWFA [22].....9

Figure 1.4: Self-injection in LWFA [22] 10

Figure 1.5: Orbits of self-injected electrons in an evolving bubble [21] 14

Figure 1.6: Temporal propagation of laser intensity [21] 17

Chapter 1: Introduction

1.1 History of plasma-based accelerators

It was first proposed by Tajima and Dawson in 1979 [1] that plasma-based accelerators could be used to generate electrons with relativistic energy by exciting plasma waves. Since that time, there have been numerous works in this field both theoretically and experimentally. With technology improvements, especially the development of petawatt, ultra-short laser system, monoenergetic electron beams with energy up to a few GeVs have been successfully generated in several experiments [2-6]. Such electron beams with ultra-high power are promising in applications including high-energy particle colliders [7] and radiation therapy in oncology [8].

The primary advantage of plasma-based accelerators is their ability to sustain high acceleration gradients. In traditional radio frequency linear accelerators, the acceleration gradients are limited to approximately 100 MV/m, due to arcing in the high voltage vacuum cavity. However, in plasma accelerators, accelerating cavity is filled with already broken down plasma, thus avoiding the vacuum arcing. In fact, ionized plasma can sustain electron

plasma waves, i. e. Langmuir waves, with electric field on the order of $E_{\parallel} = m_e c\omega_p/e$ where $\omega_p = (4\pi e^2 n_0 / m_e)^{1/2}$ is the plasma frequency, m_e is the electron mass, c is the speed of light, e is the electron charge, or

$$E_{\parallel}(V/cm) \sim 0.96 {n_0}^{1/2} (cm^{-3}) \quad (1.1)$$

where n_0 is the ambient electron density. For $n_0 = 10^{18} cm^{-3}$, $E_{\parallel} \sim 100\ GV/m$, which is several orders of magnitude greater than a conventional RF accelerator

There are several acceleration schemes proposed and widely explored in history, see Fig. 1.1. In all of these schemes, the accelerating driver travels through a plasma creating a plasma wake, which co-propagate with the driver in near the speed of light. Thus it is possible that electrons in the wake can be accelerated to relativistic energies.

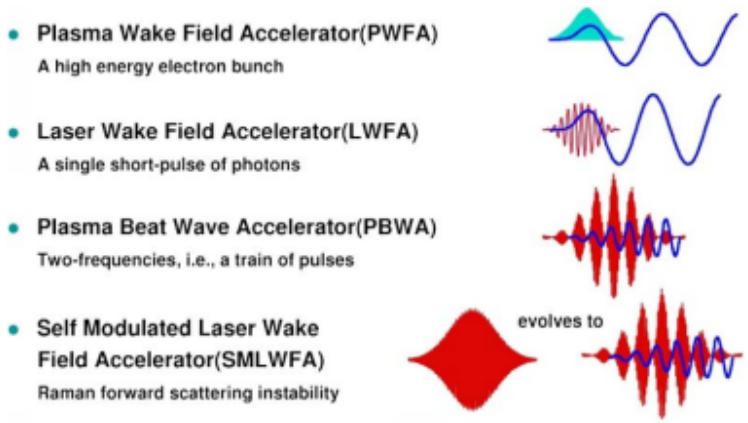

Figure 1.1: Schemes of four basic plasma-based accelerators, cited from [19]

The first proposed acceleration scheme is the laser wakefield accelerator (LWFA) by Tajima and Dawson, within which a single ultra-high intensity laser pulse is employed to excite plasma wave. However, efficient single pulse driving requires the pulse duration $\tau_L \sim \lambda_p$, where $\lambda_p = 2\pi c / \omega_p$ is the plasma wavelength. Due to technology limitations, such short, high-intensity laser pulse was not accessible at that time. Therefore, an alternative driving scheme with more feasibility, the plasma beatwave accelerator (PBWA) [1, 9], was invented. It is until in the mid 1990s that LWFA was reconsidered and further analyzed, benefiting from the development of chirped-pulse amplification and terawatt laser system.

In the PBWA, two long laser pulses with frequency difference $\Delta\omega \sim \omega_p$ are employed. In this structure, resonant plasma wave is generated by the beatwave of the two pulses. Each beat's duration in the beatwave is ω_p, satisfying the resonant excitation requirement. In the laboratory, the plasma wave generation in the PBWA is first observed by Clayton *et al.* [10] in 1985 and electron acceleration was first detected by Kitagawa *et al.* [11] in 1992. These experiments employed two lines of a CO_2 laser, traversing through a plasma with density $n_0 \sim 10^{17}\mathrm{cm}^{-3}$ and accelerating plasma to an energy of 10 MeV.

The self-modulated laser wakefield accelerator [12, 13] (SM-LWFA) also drives plasma with short powerful laser pulses, similar to LWFA. However, in SM-LWFA, the train of short laser pulses comes from a single long pulse through self-modulation instability. Compared with LWFA, SM-LWFA drives originally with a long pulse in more dense plasma, leading to $P > P_c$, where P is laser power and P_c is critical power for relativistic focusing. This condition allows laser pulse to periodically focus and diffract as the pulse travels in the plasma. Instability keeps growing and eventually breaks up the long laser into a train of short pulses. Experimental evidence

of plasma wave formed by self-modulation in high intensity plasma was first observed in 1995 [14], generating self-trapped electrons to energies ≥ 44MeV.

All these previous accelerators, such as SM-LWFA and PBWA, have demonstrated successful generation of plasma wake and relativistic electrons. However, the broad energy spread of these electron beams make them less applicable in industry. In 2002, the bubble regime was proposed by Pukhov et al. [15], which for the first time predicts quasi-monoenergetic electron beams in theory.

1.2 Driving mechanism in laser wakefield acceleration

Basically, there are types of drivers in plasma-based wakefield accelerators, intense laser pulses and charged particle beams. A laser pulse travelling through a plasma will expel plasma electrons along its propagation path by pondermotive force [20]. The expression for pondermotive force is derived by considering an electron in an oscillating electric field

$$\frac{d\mathbf{p}}{dt} = -e(\mathbf{E} + \frac{\boldsymbol{v}}{c} \times \mathbf{B}) \tag{1.2}$$

where $\mathbf{p}$ is the electron momentum, $\mathbf{v}$ is the electron velocity. $\mathbf{E}$ and $\mathbf{B}$ can be expressed with the vector potential $\mathbf{A}$ as

$$\mathbf{E} = -\frac{1}{c}\frac{\partial \mathbf{A}}{\partial t}, \mathbf{B} = \nabla \times \mathbf{A} \tag{1.3}$$

Consider the first order components in this equation, we are left with only the electric field ($\mathbf{v} \times \mathbf{B}$ is of second order nature), thus

$$\partial \mathbf{p}_1 / \partial t = -e\mathbf{E} \tag{1.4}$$

$$\mathbf{p}_1 = m_e c\mathbf{a} \tag{1.5}$$

where $\mathbf{a} \equiv \mathrm{e}\mathbf{A} / m_e c^2$ is the normalized vector potential.

The second order $\mathbf{p}_2$ can be written as

$$\frac{d\mathbf{p}_2}{dt} = -\frac{d\mathbf{p}_1}{dt} - m_e c\left[-\frac{\partial \mathbf{a}}{\partial t} + \frac{\mathbf{p}_1}{m_e} \times (\nabla \times \mathbf{a})\right] \tag{1.6}$$

$$= -\left(\frac{\mathbf{p}_1}{m_e} \cdot \nabla\right)\mathbf{p}_1 - c\mathbf{p}_1 \times (\nabla \times \mathbf{a})$$

Replaced $\mathbf{p}_1$ in the above equation with the expression of the vector potential $\mathbf{a}$, we have

$$\mathbf{F}_p = \frac{d\mathbf{p}_2}{dt} = -\frac{m_e c^2}{2}\nabla |a|^2 \tag{1.7}$$

Referring to this expression, the pondermotive force is inversely proportional to the gradient of the electromagnetic energy density,

regardless of the sign of the particle it exerts on. Therefore, particles will be pushes away from high intensity laser to lower intensities. In other words, pondermotive force of the laser pulse will expel particles out of its propagation path.

Assume a small perturbation in density $\Delta n = n_1 \cos(k_p z - \omega_p t)$ ($n_1 \ll n_0$, n_0 is the background plasma density). By integrating Poisson's equation, we have the electric field oscillation as

$$\Delta E = -E_0 \frac{n_1}{n_0} \sin(k_p z - \omega_p t) \tag{1.8}$$

The relationship of the electric field and plasma density oscillations is illustrated in Fig. 1.2.

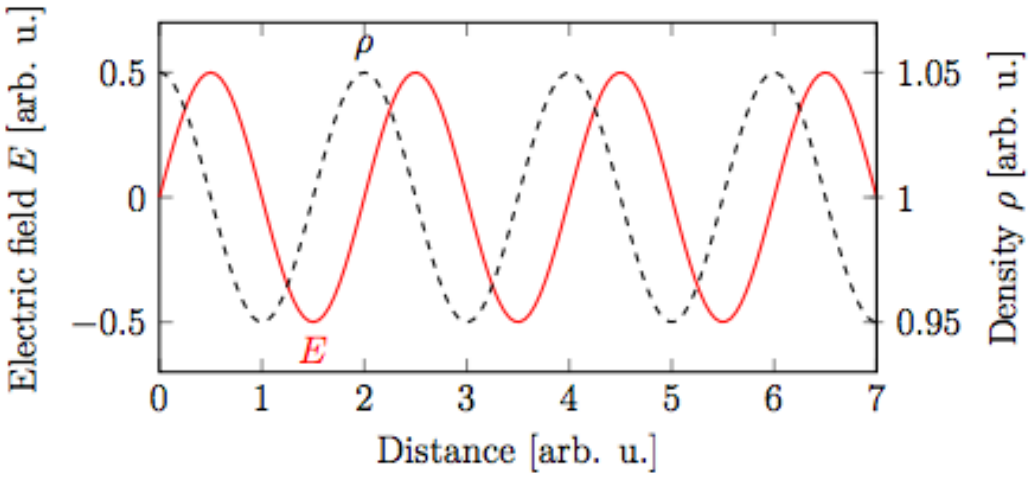

Figure 1.2: The electric field follows plasma density modulation delayed by half plasma wavelength, cited from [22]

With high intensity laser pulse, electrons will be completely expelled, leaving a plasma wave in the wake of the laser. The lack of electrons in the wake of the laser pulse will give rise to strong longitudinal electric field which can efficiently accelerate electrons in the wake. Recent experimental observations have proved that for a terawatt laser pulse used in the laser wakefield accelerator, electrons can be accelerated to several GeVs over cm distances [23].

1.3 Bubble regime formation and advantages

We have already shown that bubble is formed as driver travels through the plasma and completely expels all electrons radially, while ions are left immobile on the characteristic time scale. A blow out region (bubble) with no electron inside is created. Eventually, the expelled electrons will be attracted back to the bottom of the bubble by electric field of the left over ions, closing off the bubble structure. When electrons are born within the bubble, they may be trapped in the bubble by the deep longitudinal electric potential. This trapping mechanism allows electrons to

co-propagate with the bubble, getting accelerated to relativistic energies, as illustrated by Fig. 1.2, 1.3.

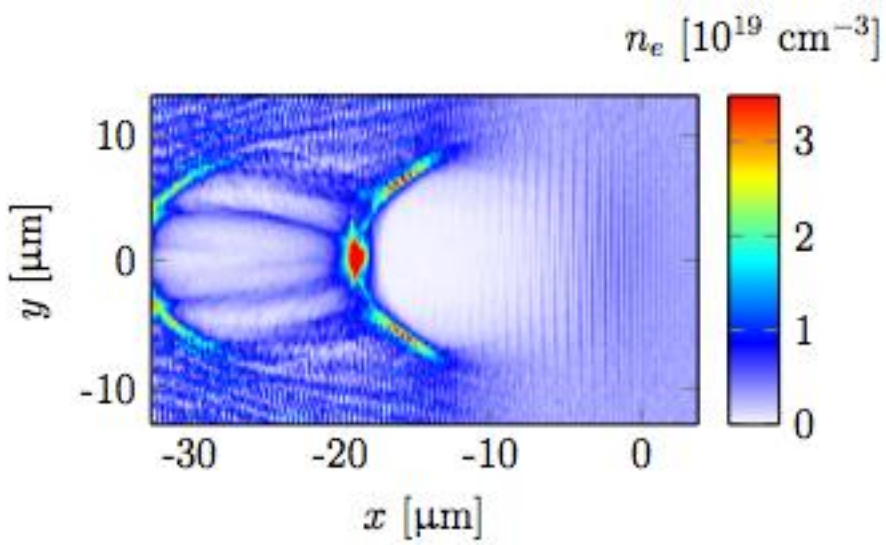

Figure 1.3: A cross section of the circular plasma wave in LWFA. Electron density cavities (bubble region) are formed behind the laser pulse, locating at $x = 0\ \mu m$. The laser is propagating in positive x-direction, cited from [22]

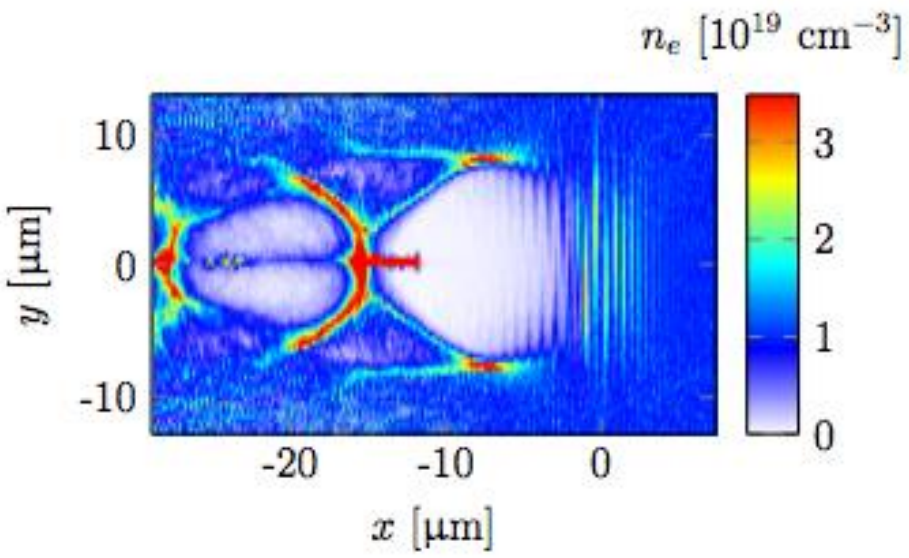

Figure 1.4: Injection due to self-injection by wavebreaking has occurred, and charge is injected in the first two plasma periods, cited from [22]

There are strict requirements on the drivers in order to fully expel all electrons and form a bubble. Ultra-short ultra-high intensity driving pulse is required. For a laser driver, the normalized vector potential $a_0 \gtrsim 1$. For a beam driver, the current must be larger than the Alfvén current. The pulse duration should be as short as plasma wavelength for resonant plasma wave excitation. Due to these limitations, the bubble regime could not be implemented in the laboratory until chirped-pulse amplification was applied to compact solid-state lasers.

Despite these experimental limitations, the bubble regime is widely adopted by most plasma-based accelerators. Compared with previous plasma-based accelerators, it has unravelled advantages as followings:

Firstly, it can generate relativistic electron beams with monoenergetic energy spectra. The bubble regime significantly improved the quality of accelerated electron beams, providing promising applications in various areas.

Secondly, instead of exciting period plasma wave, driving pulses in the bubble regime have relativistic intensities high enough to break the plasma wave after the first oscillation. Such high intensity enables the bubble structure to support much higher accelerating gradients than the conventional schemes.

Additionally, the focusing structure of the bubble regime allows for self-guiding of the laser driver and generation of collimated electron beams. The laser pulse could propagate many Rayleigh lengths (Rayleigh length $z_R = \pi\omega_0^2 / \lambda$, where λ is the laser wavelength, ω_0 is the waist size) in homogeneous plasma without a significant diffraction.

Lastly, with appropriate laser pulse and plasma density parameters, self-injection is possible, which has bright implications. With self-injection,

external injectors (such as a second laser pulse) are avoided, saving much trouble from experiment setup technically. However, self-trapping in a traditional bubble regime puts stringent requirements on parameter settings. In case of the tenuous plasma, one must have extremely large bubble size to get a single acceleration process with high gradients. Therefore, effective self-injection scheme of ambient plasma is an important part of bubble acceleration. In recent years, this topic has been intensively investigated analytically and experimentally.

1.4 Self-injection schemes

Several different self-injection models have been developed recently, based on different driver types and bubble evolvement. In each model, to get monoenergetic electron beams, the acceleration process will consist of a particle self-injection period followed by a pure acceleration period.

1.4.1 Self-injection in the temporally evolving bubble

One of the mechanisms proposed is self-injection by temporally evolving bubble [16]. In the injection period, the dynamically expanding

bubble could effectively inject and trap electrons by the deepening potential inside the bubble. It is analytically demonstrated that one important factor for self-injection is bubble expansion rate. In order to trap electrons passing through, the bubble must expand fast enough to considerably increase its radius during electrons' slippage time. It has been recently proved in theory [evolving bubble] that in order to trap an initially quiescent electron with Hamiltonian $H_{in} = H(\xi = +\infty) = 1$, change in its Hamiltonian should be greater than -1. So that $H_{fin} < 0$ and the electron will stay in the bubble permennantly. Three trajectories for trapped, passing and injected non-trapped electrons in the expanding bubble are illustrated as in Fig. 1.4, together with their Hamiltonians along the propagation distance.

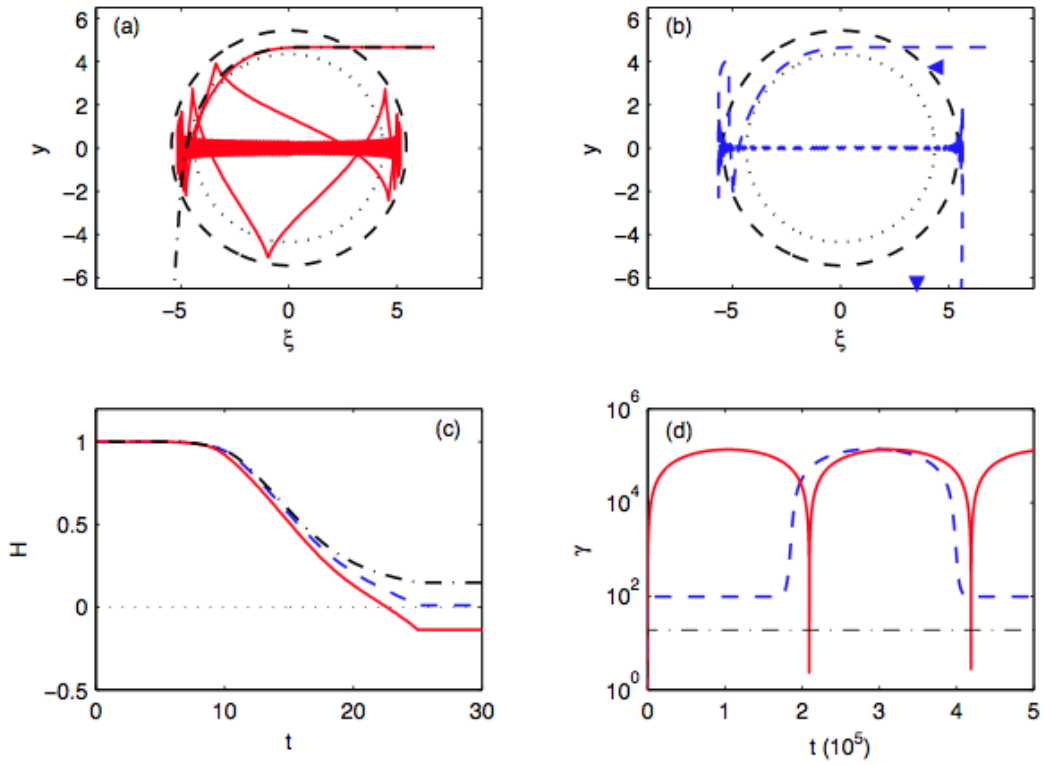

Figure 1.5: Self-injection and acceleration of electrons in the expanding bubble, simulated with WAKE code. (a) Orbits of trapped (red, solid) and passing (black, dash-dotted) electrons. (b) Orbit of an injected non-trapped electron (blue, dashed). (c) Temporal variation of the Hamiltonians. Trapped electron (red, solid) has $H_{fin} = -0.14$, injected, non-trapped (blue,dashed) has $H_{fin} = -0.01$, and passing (black, dash-dotted) $H_{fin} = 0.15$. (d) Temporal variation of electron energy. Cited from [21]

The self-injection period is terminated when the bubble stops growing. At the ending moment of the self-injection period, electrons at the head of all injected electrons are injected earlier and gain higher energy than

those in the back. However in the following pure acceleration period, the accelerating force on axis is inversely proportional to longitudinal position as $F_z \sim -\xi / 2$ [21], where ξ is the longitudinal position inside the bubble. Those on the tail of all injected electrons experience larger acceleration force and get accelerated more strongly. In this pure acceleration period, tail electrons gain more energy than head electrons. The result is the formation of a monoenergetic electron beam.

1.4.2 Field ionization induced self-injection

Another injection technique, which does not depend on bubble evolution, is the field ionization induced injection, which is the scheme employed in this thesis. This structure is first implemented and detected relativistic electron beams by Pak et al. [17]. This structure employs one element as background gas and dopes in certain area with another element, which has multiple shells and higher ionization potential. As laser driver propagates through this doping gas, electrons of the background gas and the outer shell of the dopant gas are firstly ionized and to form the blow out region. As laser intensity grows to exceed the ionization threshold for the

inner shell of the dopant gas, these inner shell electrons are then ionized. Since these electrons originated from inside of the bubble, with a negative Hamiltonian, they are well trapped in the bubble and will get accelerated with bubble phase velocity.

During the period of inner shell ionization, if both the bubble and laser driver propagate stably with little evolution, inner shell dopant electrons will continuously get injected and accelerated in the bubble. Newly injected electrons will gain less energy than the previous ones, resulting in an electron beam with broad energy spectrum. To narrow down the energy spread, the ionization injection time needs to be carefully controlled.

One method for obtaining limited ionization time is to adjust spot size of the laser pulse. Previously laser pulse spot size matches with plasma density. With such a matched spot size, the laser pulse will undergo minimum evolution during its propagation. Intensity sustains above ionization threshold leading to continuous self-injection, but with a broad energy spectrum. However if the laser spot size is mismatched with the plasma density, the laser pulse will first focus to a peak intensity that is greater than the ionization threshold, followed by a defocusing phase terminates the self-injection process. When this is the case, self-injection

only happens in a relatively short time period and then the trapped electrons undergo a pure acceleration period with high accelerating gradient. Therefore initial injection time spread is narrowed down, creating better monoenergetic electron beams.

The technique is implemented recently in a experiment in Texas Petawatt wakefield acceleration experiment and confirmed with WAKE simulations, as illustrated in Fig. 1.5.

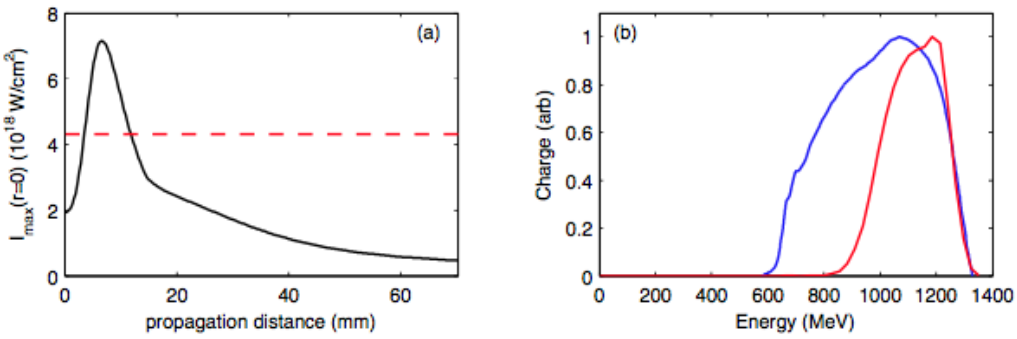

Figure 1.6: (a) Maximum laser intensity on axis as a function of propagation distance. The threshold ionization intensity for the N^{5+} ions is indicated with a red dashed line. Where the laser is greater than the threshold intensity, ionization injection is expected to occur. (b) Experimental (blue) and simulated (red) electron energy spectra. Cited from [21

In the experiment, background plasma is doped with the N^{5+} ions of Nitrogen. As illustrated by Fig. 1.5, ionization induced injection only occurs near the beginning of the propagation. Injection is then terminated by laser

diffraction roughly around 15 mm. Electrons can be accelerated to approximately 1 GeV with relatively narrow energy spread.

In order to obtain high energy for the accelerated electrons, it is necessary to access the self-guided blowout regime for higher accelerating fields and longer acceleration distance. Estimation of the self-guided intensity is as follows.

During the self-guided stage, diffraction is balanced with relativistic self-focusing. The matched spot size is given by [24]

$$k_p \omega_0 \approx 2\sqrt{a_0} \tag{1.9}$$

The power for relativistic self-focusing is [25]

$$\frac{P}{P_c} = \frac{1}{32}\left(k_p \omega_0\right)^2 a_0^2 \tag{1.10}$$

where P_c is the critical laser power. Therefore, we can estimate self-guided intensity as

$$a_0 \approx 2\left(\frac{P}{P_c}\right)^{\frac{1}{3}} \tag{1.11}$$

For relativistic self-focusing laser pulse, $P/P_c > 1$. Thus $a_0 \gtrsim 2$ is required for a self-guided laser.

However, for accelerating with the self-guided pulse, we need to be careful in choosing the type of dopant gas regarding their ionization threshold. The threshold for the inner shell of dopant gas should be larger than the self-guided intensity. Otherwise it will result in continuous injection in the self-guided period.

An alternative method to narrow down electrons' energy spread is to control the size and position of the dopant gas located within the background gas, which is the situation studied in this thesis. By adjusting the dopant gas position and size, we can conveniently change the time and duration for ionization injection, thus controlling the quality and energy spread of accelerated electron beams. By carefully choosing the pulse intensity, electron ionization will only occur at the peaks in each laser period, resulting in pulsed injection in phase space. Since the bubble moves nearly in same phase velocity with the laser pulse, this discrete pattern will not be disturbed as the bubble propagates. Due to the trapping dynamics in the highly nonlinear bubble region, these initially discretely injected electrons will be matched to the discrete trapped electrons at the bottom of the bubble [18]. This electron bunching structure is the primary focus of this thesis.

1.5 Summary

In summary, the plasma-based accelerator is a promising scheme for the development of compact electron accelerators. Compared with traditional accelerators, it can support much higher acceleration gradient. Acceleration drivers, either a laser pulse with pulse length around plasma wavelength, or a beam of charged particles, travel through the plasma, exciting Langmuir waves. Electrons "ride" on these plasma waves, co-propagate with the wave and get relativistically accelerated. There have been several driving schemes proposed in history, namely LWFA, PWFA, PBWA and SM-LWFA. With development of chirped pulse amplification, ultra-high intensity, short pulses became accessible. The bubble regime is proposed and became the acceleration schemes in the majority of modern plasma-based accelerators. For generating monoenergetic electron beams in the bubble region, the self-injection process plays an important role. In the field ionization self-injection mechanism, electrons trapped in the back of the bubble produce bunching pattern under certain parameter settings. Such bunched electron beams have a bright potential for the generation of high-intensity ultraviolet radiation.

The following chapters present simulations by the quasi-static PIC code WAKE and theoretical analysis. Various factors affecting electron bunching are investigated and analytical reasoning is provided.

Chapter 2. Electron bunching in ionization induced self-injection

2.1 The high-frequency laser pulse driver and self-injected electrons

In this thesis, we consider the ionization induced injection in laser wakefield accelerators. A single laser pulse is adopted for creating the bubble and ionizing electrons inside. In earlier works in WAKE, laser field ionization is performed without considering the high-frequency oscillations of the laser pulse as shown in Fig. 2.1(a), thus injected electrons are distributed nearly uniform in the area with field above ionization threshold. However, to obtain the bunching phenomenon for trapped electrons, we need finer structure of the laser pulse for initial phase space discretization of injected electrons. In the following simulations, electric field of the laser pulse is modulated by an oscillating factor $\exp(-i\omega_0\xi / \omega_p)$, where ω_0 is the laser frequency, ω_p is the plasma frequency, $\xi \equiv z - v_0 t$ is the longitudinal phase space position and v_0 is the phase velocity of the wake. Fine-structured laser pulse is plotted as Fig. 2.1(b).

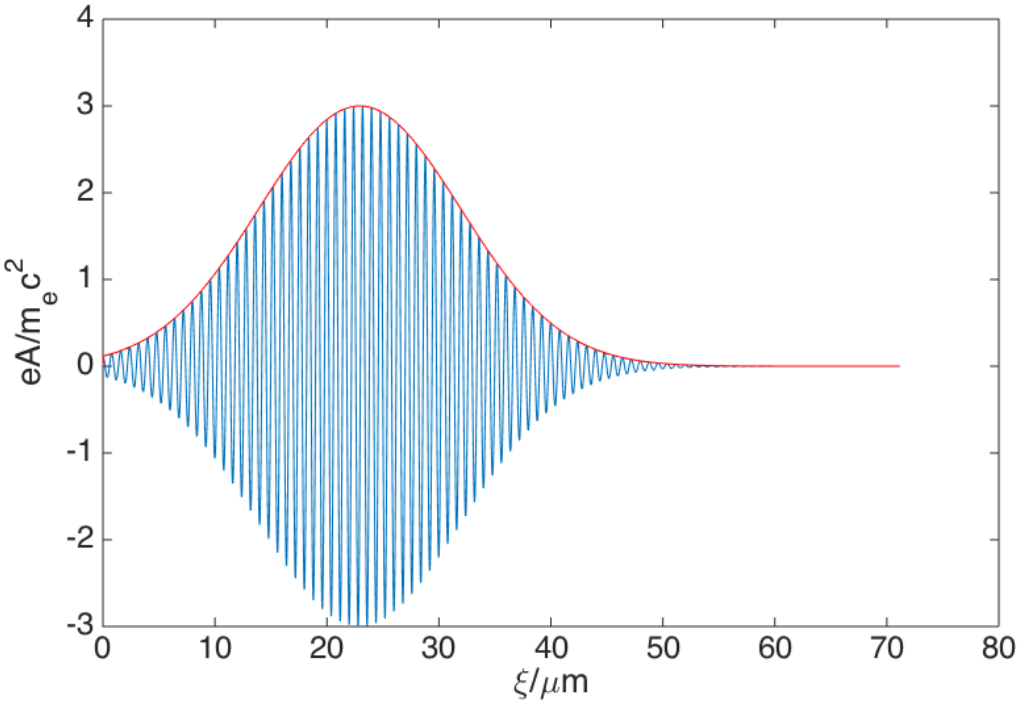

Figure 2.1: Profile of an 800nm laser pulse's intensities on the axis of the simulation window in WAKE. The x-axis represents position along the longitudinal direction in the simulation box, while the y-axis represents the normalized vector potential for electromagnetic field of the laser pulse. Previous code only depicted the envelope of the laser pulse without high-frequency details (red line). Upgraded code includes the high frequency oscillations of the laser pulse (blue line).

It is important in the simulation that peaks of the oscillating laser pulse should perfectly follow the expected intensity envelope, since the ionization injection in this thesis are localized to the small peak area of the laser pulse. One thing worth noticing in the WAKE code is that, an appropriate longitudinal grid size $\Delta\xi$ is crucial for simulating a smoothly oscillating laser pulse. In order to depict each peak of the high-frequency

pulse without losing too many details, it is necessary to define a small grid size. In the case of a laser pulse with wavelength $\lambda_L = 0.8\mu m$ and pulse duration $\tau_L = 50$fs, two plots with different longitudinal grid size $\Delta\xi$ are shown below as Fig. 2.3.

In such an appropriately defined high-frequency laser pulse, electrons are injected only in the peaks and troughs of the oscillating laser field, resulting in an initial discrete injection pattern in phase space.

We depicted the initial injection plot for an 800 nm laser pulse with normalized peak intensity $a = 3.71$, duration $\tau_L = 50$fs and spot size $w_0 = 20\mu m$, dopant gas ionization threshold is 3.60. Fig. 2.2 proves that ionization injection happen around peaks of the laser pulse and injected electrons spaced by half laser wavelength.

For more accurate injection simulation, we also introduce finer grid in the transverse direction to WAKE code. In order to keep the code from being too time-consuming, transversely fine grid is only defined in the ionization injection sector. One thing worth noticing is that when defining the fine grids for laser electric field by interpolation, field vectors on the two transversely adjacent grids will almost cancel out. So that interpolation should be conducted on the absolute amplitude of laser electric field.

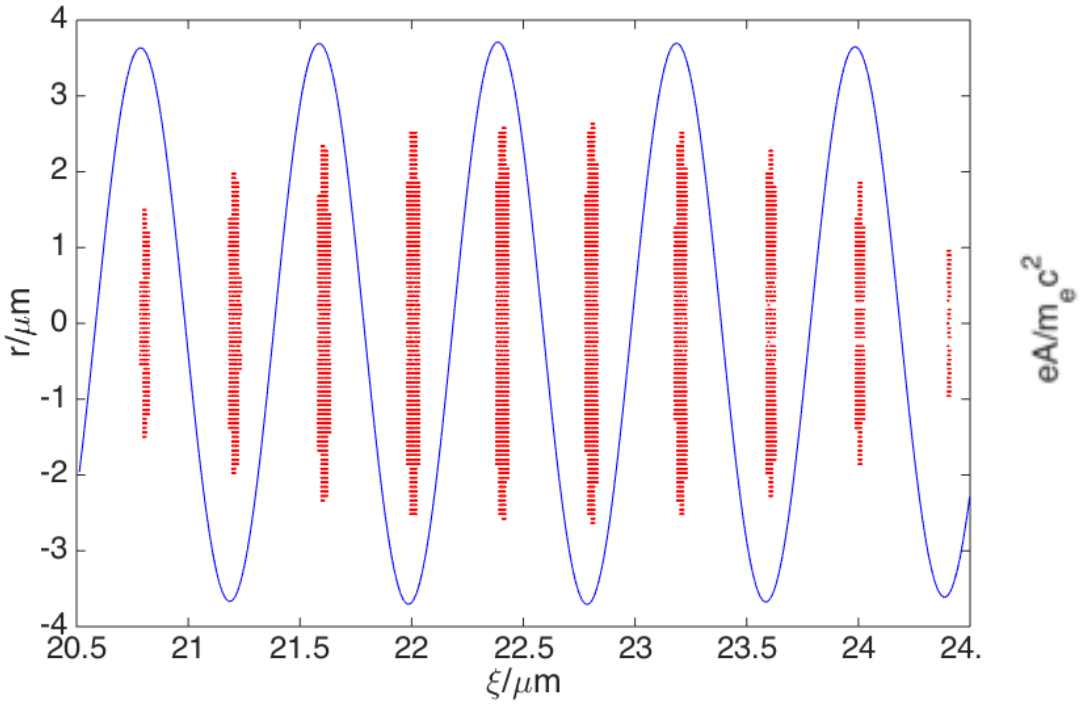

Figure 2.2 Electrons' injection distribution in the cross section of the cylindrically symmetric simulation box. The laser pulse propagates along negative ξ direction. The left y-axis with $r(-4\mu m, 4\mu m)$ represents the radial position, while the right y-axis is the normalized vector potential for the driving laser pulse The red dots are the initial ionization position for self-injected electrons. The solid blue line is the laser intensity on axis ($r = 0$). We can see that electrons are ionized on each peak of the laser pulse. Each injected electron bunch is separated by half laser wavelength.

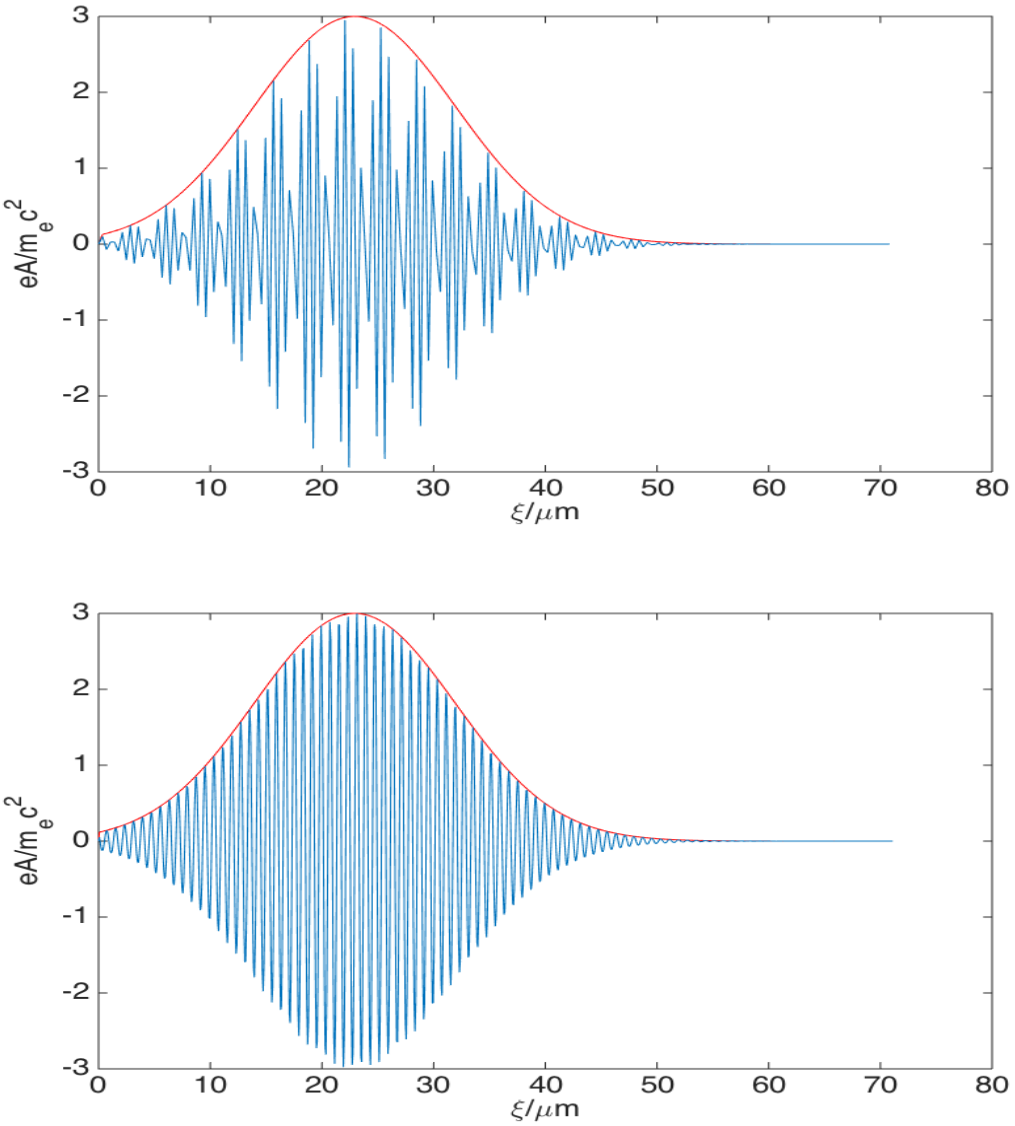

Figure 2.3: Profiles for laser pulse intensities on axis (r = 0) in the simulation box with different grid size $\Delta\xi$. The x-axis indicates the longitudinal position in the cylindrically symmetric simulation box, whereas the y-axis is the normalized vector potential of the laser field. The red line is the expected peak intensity envelope. The blue line is the actual laser intensity profile simulated in the WAKE code. Top plot: Laser profile with longitudinal grid $\Delta\xi = 356\,nm$. We can see that with relatively large grid, actual laser peaks (blue line) will not smoothly follow the peak envelope (red line). A lot of details are lost. Bottom plot: Laser profile with longitudinal grid $\Delta\xi = 71\,nm$. The simulated laser (blue line) depicts most part of the expected laser envelope (red line), yet still loses some details for laser pulse peaks with highest intensities.

2.2 Parameters for laser driver and simulation domain

In the following WAKE simulations, an 800 nm laser pulse with normalized vector potential $a_0 = 3$, duration $\tau_{\mathrm{FWHM}} = 50\mathrm{fs}$ propagates into a mixture of pre-ionized plasma and a certain type of ions. ξ is the propagation direction. Simulation box in the WAKE code is cylindrically symmetric, so that the simulation domain (ξ, r) half of the cross section along the axis of the circular cylinder. Domain's dimensions are $71.2\mu m \times 119.8\mu m$ with 400×5000 cells, corresponding to grid size $0.1779\mu m \times 0.0240\mu m$. Particularly in the ionization injection time, grid size is redefined in the transverse direction and reduced to $0.1779\mu m \times 0.0048\mu m$.

2.3 Electron trapping dynamics in the highly nonlinear bubble

The electron trapping process in the bubble regime can be roughly divided into three stages.

Electrons are born at the front of the bubble and move towards the back of the bubble, getting accelerated relativistically by electric field in the wake

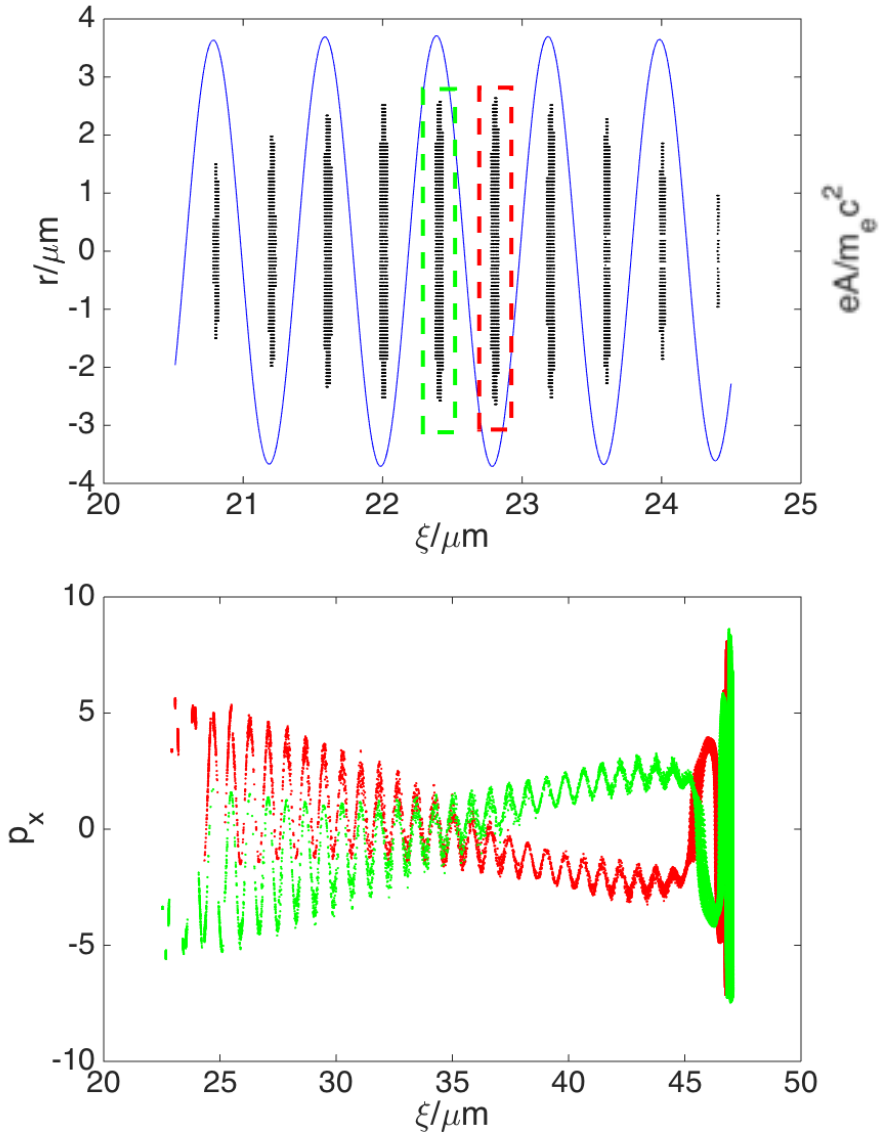

Figure 2.4: Top graph: One snapshot of the cross section in the cylindrically symmetric simulation box with ξ as the longitudinal axis and r as the transversal axis. The snapshot is taken immediately after electrons (black dots) are born in the bubble. The right y-axis indicate normalized vector potential for the laser pulse. The laser intensity on axis ($r = 0$) is also plotted in the blue line. Bottom graph: The propagation of radial electron momentum p_x is plotted against its longitudinal position ξ in the bubble. Electrons are sampled from the two electron slices on the top graph, marked with dashed windows (green and red). From each window (green and red), we have chosen ~100 electrons with extremely small spread in ξ ($\Delta\xi \ll 1$). The laser pulse center is located at $\xi \approx 22.4\mu m$ with FWHM~15μm

For stage 1, when electrons are born at the head of the bubble by laser field ionization, they will experience much higher electromagnetic field from the laser pulse than the wakefield. Thus the laser field dominates this stage, leading to electron momentum oscillating in phase with the laser pulse, as shown by Fig. 2.4 above.

For stage 2, electrons slip away from the laser pulse and move towards the back of the bubble.

For stage 3, as electrons finally get trapped in the back of the bubble and accelerated to relativistic energy, we can analyze its motion by Hamiltonian conservation.

Under the quasi-static approximation, the Hamiltonian $H = \gamma - v_0 p_z - \Phi$ is conservative, where $\gamma = \sqrt{1 + p_r^2 + p_z^2 + a^2}$, Φ is pseudo potential. In the model of a spherical bubble, $\Phi = -(\xi^2 + r^2)\omega_p^2 / 4c^2$. Here ξ and r are the longitudinal and transverse position in cylindrically symmetric phase space of the bubble region and c / ω_p is the plasma skin depth. By the conservation of Hamiltonian and noticing that initially $H = 1 - \Phi$, the longitudinal position of the trapped electron in phase space is [18]

$$\xi = \sqrt{4 + \left(\frac{\xi_i^2 + r_i^2 - r^2}{c^2}\right)\omega_p^2 - 4(\gamma - v_0 p_z)} \qquad (2.1)$$

If ionization threshold is extremely close to the maximum laser pulse intensity, only a small amount of electrons will be ionized in the area localized at the center of the laser pulse ($r_i \ll 1,\ p_r \ll 1$). Also at the back of the bubble, electrons are accelerated to relativistic energy, $(\gamma - v_0 p_z) \ll 1$. Thus final trapping position $\xi \approx \sqrt{\frac{4c^2}{\omega_p^2} + \xi_i^2}$ [16], only depends on the initial injection position ξ_i. Theoretically it demonstrates that bunching is preserved from initial to the final phase space. Electron in the same injection sheet (same ξ_i) will eventually end up in the same trapping sheet (same ξ).

The following fig. 2.4 displays the bunching of initial injected and final trapped electrons in the bubble, with the same laser driver described in Section 2.1. The background plasma density is $n_0 = 1.81 \times 10^{18}\text{cm}^{-3}$, ionization injection begins when laser propagation distance is 0.626 mm.

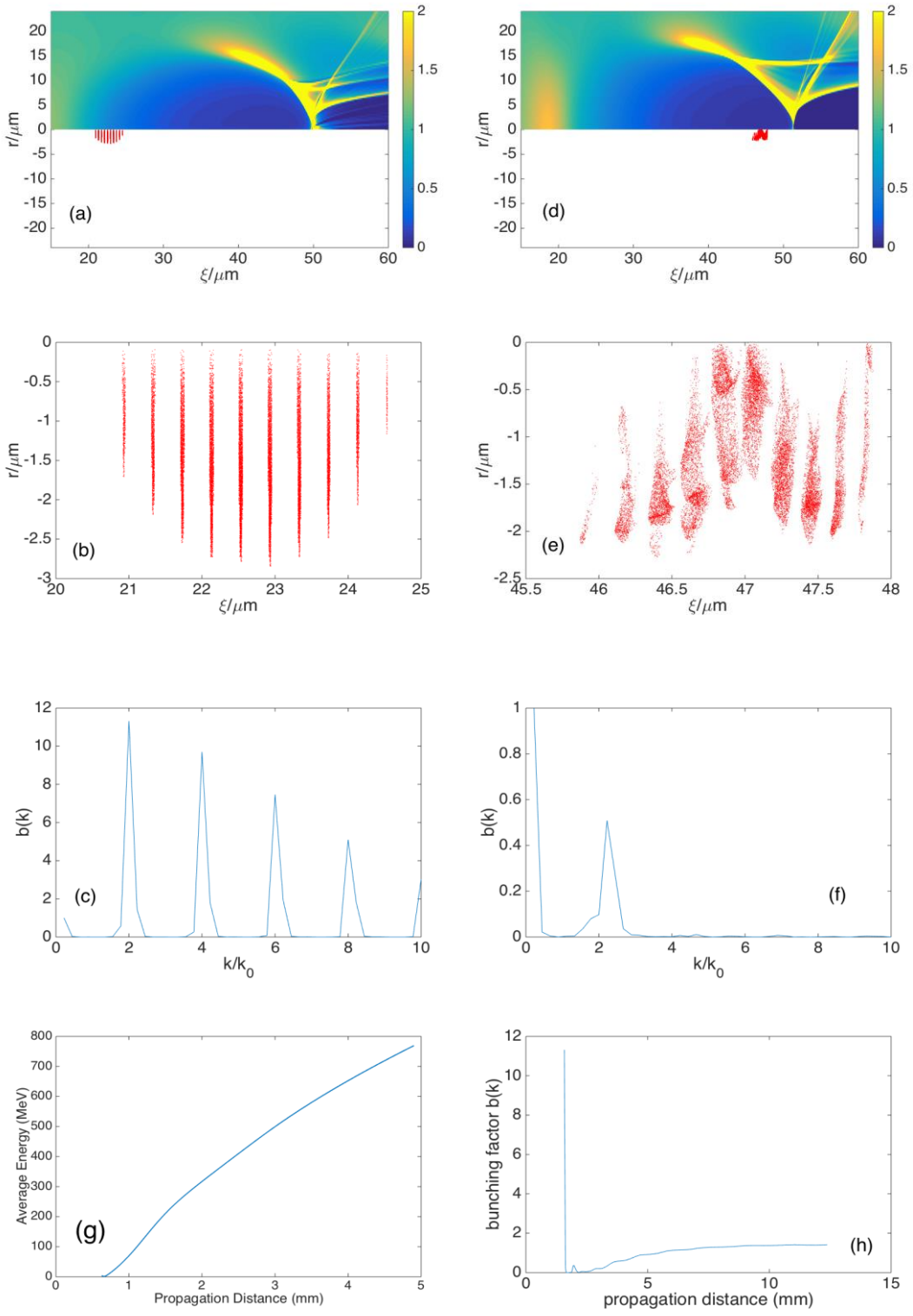
(a)
(b)
(c)
(d)
(e)
(f)
(g)
(h)
r/μm
ξ/μm
b(k)
k/k0
Average Energy (MeV)
Propagation Distance (mm)
bunching factor b(k)
propagation distance (mm)

Figure 2.4

Figure 2.4 (a) and (d) are snapshots in the cross section of the cylindrically symmetric simulation box. The upper half cross sections are density distributions for the background electrons in the plasma. The spherical blue area depicts the bubble region. The lower half cross sections plot the position of seeded test particles in red dots. Dots in (a) are the initially injected electrons at the front of the bubble with propagation distance $z = 0.626mm$. Dots in (d) are the relativistic electrons finally trapped in the back of the bubble with propagation distance $z = 3.131mm$. (b) and (e) are zoomed in pictures of the injected electrons in (a) and (d). (c) and (f) are bunching factor plots for density modulation in these electrons at propagation distance $= 0.626mm$ and $z = 3.131mm$. Bunching factor scale for (c) is (0,12) while for (f) is (0,1). (g) Averaged electron energy plotted against the propagation distance. Estimated bubble energy $\gamma \sim \frac{1}{\sqrt{3}}\frac{\omega_p}{\omega_0} \approx 17.93$. Thus electron trapping occurs at approximately propagation distance $z \approx 0.783mm$. (h) The amplitude of bunching factor b(k) for the first non-trivial peak in injected electron density distribution, plotted against the propagation distance. As you can see, after electrons get trapped at $z \approx 0.783mm$, bunching quality gradually improved to a significant level.

From Fig 2.4 (b) (e), we can see that initial injected electron sheets are separated by $0.4\mu m$, exactly half laser wavelength, while trapped electron sheets' separation is clearly suppressed, resulting in a larger wavenumber. This is also clear in the Fourier transformation of electron density profiles as in Fig. 2.4(c) (f). On these graphs, k / k_0 is the normalized modulation wavenumber and $b(k) = \left|\int d\xi_f \exp\left(ik\xi_f\right) \mathrm{g}\left(\xi_f\right)\right|$ is the bunching factor for corresponding modulation. (The distribution of longitudinal final positions ξ_f is $\mathrm{g}\left(\xi_f\right)d\xi_f = d\xi_i \int dr_i f(r_i, \xi_i)$ where r_f is neglected for high energy electrons) Initially the second harmonic is at $2k_0$ and moves to $\sim 2.22k_0$ at the trapping time.

Through conservation of the Hamilton and Fourier analysis, it can be theoretically derived [18] that in the density profile for trapped electrons, the strongest wavenumber, normalized by the wavenumber of the injection laser k_0, can be expressed roughly as:

$$\frac{k}{k_0} = 2h_m = 2\sqrt{\frac{4c^2}{\omega_p^2} + \bar{\xi}_\iota^{\,2}}/\left|\bar{\xi}_\iota\right| \tag{2.2}$$

Here $h_m = \sqrt{4c^2 \,/\, \omega_p^2 + \bar{\xi}_\iota^{\,2}}/\left|\bar{\xi}_\iota\right|$ is the wavenumber shift factor obtained from the nonlinear mapping process, while the factor 2 comes from the ionization process. $\bar{\xi}_\iota$ is the average electron ionization position, relative to the center of laser potential contour, as shown in Fig. 2.7. The plasma skin depth is $c \,/\, \omega_p$.

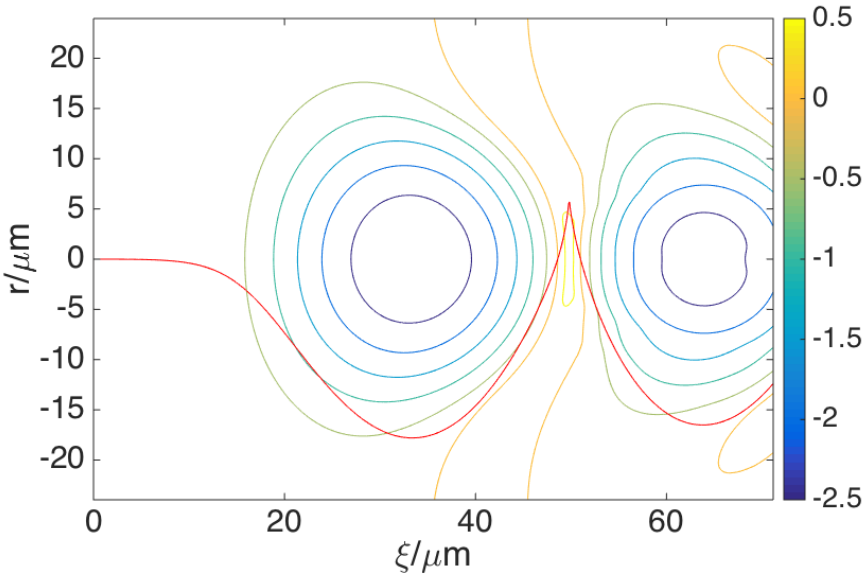

Figure 2.7: Laser potential contour (circles with color from blue to yellow, amplitude is shown in the right colorbar) at the propagation distance $z = 0.626mm$, which is the beginning of ionization injection. The window is a cross section of the cylindrically symmetric plasma simulation box. The potential is roughly in a circular shape. Referring to the potential on axis ($r = 0$) (red line), the deepest potential locates at $\xi \approx 33.6\mu m$.

In case of the ionization injection in Fig. 2.4, averaged ionization position $\bar{\xi}_i' = 22.62\mu m$, compared with the deepest laser potential point $\xi_p = 33.6\mu m$ obtained from Fig. 2.7, we have $\bar{\xi}_i = \left(\xi_p - \bar{\xi}_i'\right) \approx 10.08\mu m$, with the plasma skin depth $c\,/\,\omega_p = 3.95\mu m$. Referring to equation (2.2), $k\,/\,k_0 \approx 2.45$, roughly consistent with our simulation result of 2.24. The discrepancy may be due to laser potential shape not perfectly described.

2.4 Conditions for effective electron bunching

For effective electron bunching, any electron with the same initial position ξ_i should be mapped to the same final position ξ with littlte spread. According to Eq. (2.1), for a fixed ξ_i, the spread in ξ comes from spreads in r_i, r and $\gamma - v_0 p_z$. Fig. 2.5 shows the (p_z, ξ) distribution for electrons in one center injected sheet at $z = 0.626mm$.

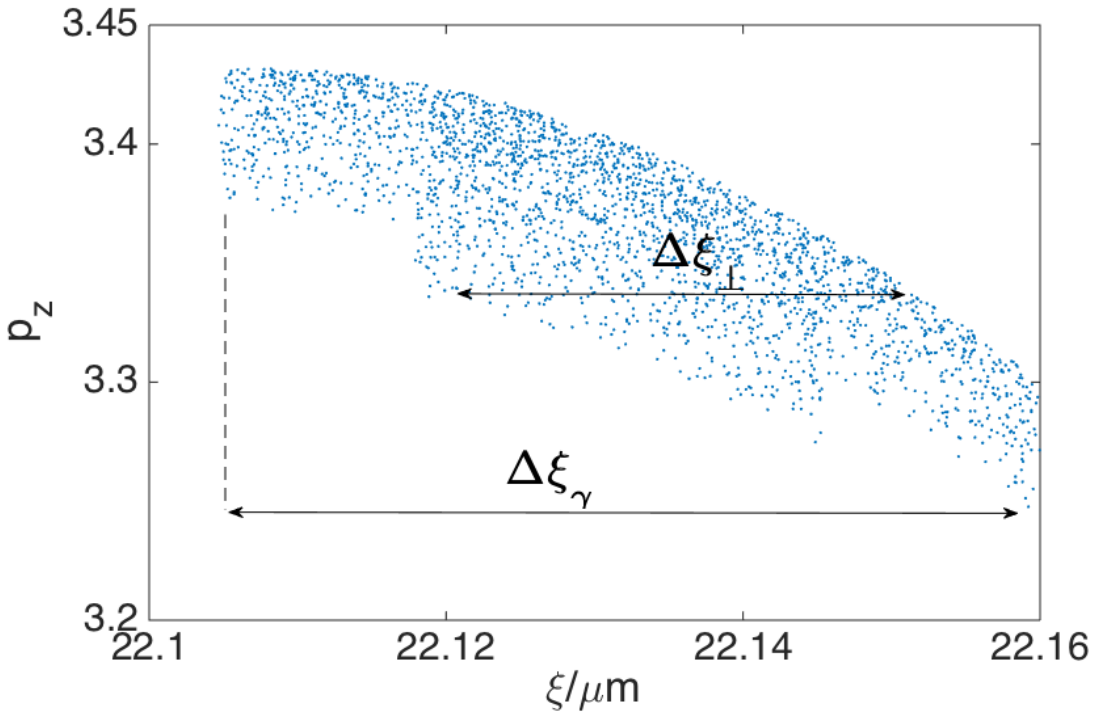

Figure 2.5 (p_z, ξ) phase space distribution for injected electrons in one peak of the laser pulse (close ξ_i, $\Delta\xi_i \approx 0.05\mu m \ll \lambda_L$), where p_z, is the electron's longitudinal momentum and ξ is the longitudinal position in the bubble. $\Delta\xi_\perp$ is the longitudinal position spread due to transversal momentum and $\Delta\xi_\gamma$ is the spread due to the energy spread.

$\Delta\xi_\perp$ is due to the motion in transverse direction, while $\Delta\xi_\gamma$ is due to the energy spread in this electron sheet. By theoretical works of Xu el. at [18], $\Delta\xi_\gamma$ can be controlled by controlling ionization duration L_{inj}. Electrons injected earlier at the same ξ_i will gain higher energy, thus longer ionization duration will result in wider energy spread.

Another factor critical to the bunching is the radial spread of injected electrons within the bubble. Electrons with larger initial r_i (further apart from the axis) will introduce in larger ξ spread in final space. Therefore, we need to limit the ionization threshold close to maximum laser intensity so that ionization only occurs at the small center area of the laser pulse. Also the spot size of the laser pulse should be carefully chosen. We need to have smaller spot size while not too small to effectively excite the bubble.

In conclusion, to get better bunched electrons, we can shorten the ionization duration, control the injection laser intensity and limit the laser spot size. This is consistent with WAKE simulation as shown in Fig. 2.6.

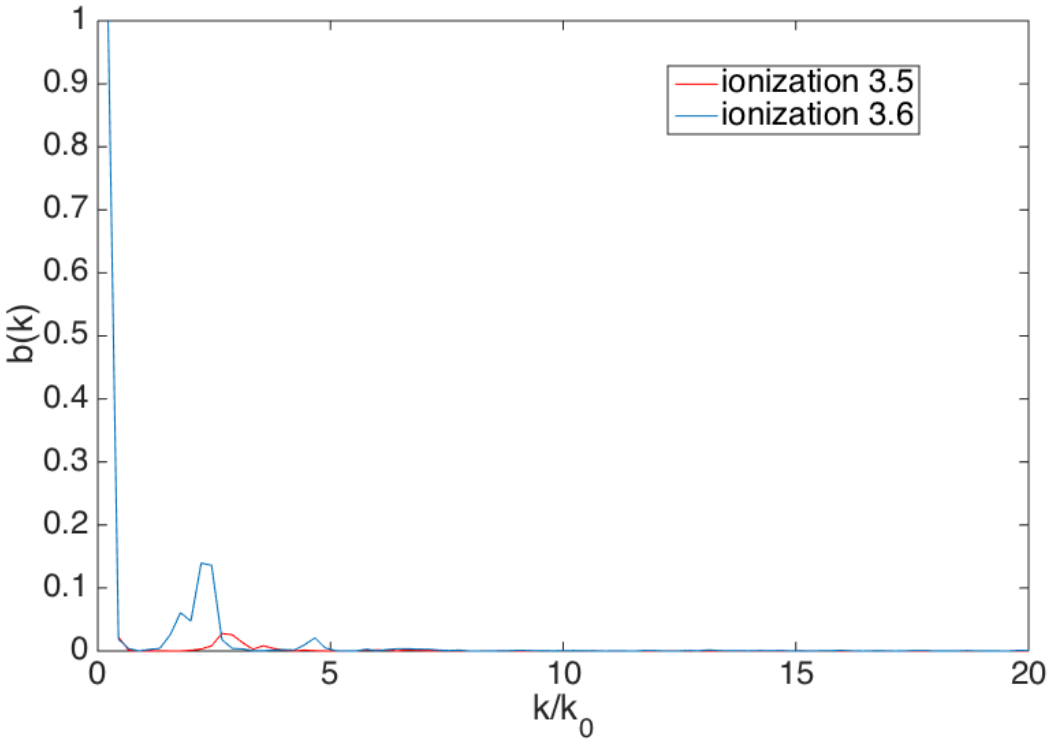

Figure 2.6: Bunching factor plots for trapped electrons with 2 different ionization thresholds, positioned at $z = 1.096mm$

All other parameters in Fig. 2.6 are the same except for ionization threshold. In one case, normalized ionization threshold is 3.5 while in the other is 3.6. The laser intensity is 3.7 at injection time. Fig. 2.6 plots the bunching factor graph for the above two cases. It is clear that bunching factor for second harmonic is significantly larger for ionization threshold

closer to the laser intensity. This result may implicate electron bunching is extremely sensitive to the ionization threshold. With slightly lower threshold, the electrons born off the bubble axis will greatly affect the spread of final trapping pattern and reduce the quality of electron bunching.

Chapter 3. Summary

In the past few decades, plasma-based accelerators have attracted considerable attention in its ability to produce ultra-high acceleration fields. Most modern plasma-based accelerators are produced in the bubble regime. Self-injection is a critical process for electron acceleration in the bubble regime. This thesis has focused on the electron bunching phenomenon in the ionization induced laser wakefield accelerator.

The self-injection and acceleration process has been simulated in a quasi-static PIC code WAKE. We upgraded WAKE to enable ionization self-injection by laser drivers with high-frequency oscillations. Higher resolution for the simulation box is defined in order to obtain an accurate electron distribution pattern. For keep to code from too time-consuming, transversal grid size is decrease only in the part of test particle seeding.

We achieved self-injected electron beams with low emittance in laser wakefield accelerators, by controlling the ionization threshold only slightly below the intensity in the driving laser pulse. Accelerated electrons' bunching phenomenon is analyzed quantitatively by using the Fast Fourier Transformation. The density modulation in the accelerated electrons have

been analyzed and confirmed with theoretical models. It has also been verified that shorter ionization duration, closer ionization threshold to laser intensity and smaller laser spot size will increase the quality of electron bunching. In particular, the quality of electron bunching may be very sensitive to ionization threshold variance.

References

[1] T. Tajima and J. M. Dawson. *Phys. Rev. Lett.*, **43**:267, 1979.

[2] W. P. Leemans, B. Nagler, and A. J. Gonsalves *et al. Nature Phys*., **2**:696, 2006.

[3] S. Karsch, J. Osterhoff, and A. Popp *et al. Nature Phys*., **9**:415, 2007.

[4] N. A. Hafz, T. M. Jeong, and I. Choi *et al. Nature Photonics*, **2**:571, 2008.

[5] J. Osterhoff, A. Popp, and Zs. Major *et al. Phys. Rev. Lett*., **101**:085002, 2008.

[6] S. Kneip, S. R. Nagel, and S. F. Martins *et al. Phys. Rev. Lett*., **103**:035002, 2009.

[7] A. Caldwell *et al. Nat. Phys*., **5**:363, 2009.

[8] K. R. Hogstrom and P. R. Almond. *Phys. Med. Biol*., **51**:R455, 2006.

[9] M. N. Rosenbluth and C. S. Liu. *Phys. Rev. Lett*., **29**:701, 1972.

[10] C. E. Clayton, C. Joshi, C. Darrow, and D. Umstadter. *Phys. Rev. Lett.,* **54**:2343, 1985.

[11] Y. Kitagawa, T. Matsumoto, T. Minamihata, K. Sawai, K. Matsuo, K. Mima, K. Nishihara, H. Azechi, K. A. Tanaka, H. Takabe, and S. Nakai. *Phys. Rev. Lett*., **68**:48, 1992.

[12] N. E. Andreev, L. M. Gorbunov, V. I. Kirsanov, A. A. Pogosova and R. R. Ramazashvili. *Pis'ma Zh. Eksp. Teor. Fiz*., **55**:551, 1992.

[13] Jr. T. M. Antonsen and P. Mora. *Phys. Rev. Lett*., **69**:2204, 1992.

[14] C. A. Coverdale, C. B. Darrow, C. D. Decker, W. B. Mori, K-C. Tzeng, K. A. Marsh, C. E. Clayton, and C. Joshi. Phys. Rev. Lett. **74**:4659, 1995.

[15] A. Pukhov and J. Meyer ter Vehn. *Appl. Phys. B*, **74**:355, 2002.

[16] Kalmykov, S. *et al. Phys. Rev. Lett*., **103**:135004, 2009

[17] A. Pak *et al. Phys. Rev. Lett*., **104**:025003, 2010.

[18] X. L. Xu, C. J. Zhang, F. Li, Y. Wan, Y. P. Wu, J. F. Hua, C.-H. Pai, W. Lu, W. An, P. Yu, W. B. Mori, and C. Joshi. *arXiv preprint arXiv*, **1510**:01445, 2015.

[19] C. Huang, V. K. Decyk, C. Ren, M. Zhou, W. Lu, W. B. Mori, J. H. Cooley, T. M. Antonsen Jr., T. Katsouleas. *Journal of Computational Physics*, **217**:658021, 2006.

[20] K. L. F. Bane, P. Chen, and P. B. Wilson. *IEEE Transactions on Nuclear Sci*., **NS -32**:3524, 1985.

[21] S. Yi, *"Injection in plasma-based electron accelerators",* 2012.

[22] E. Henrik, *"Parametric study of density down-ramp injection in laser wakefield acceleration"*, 2015.

[23] W. Leemans, A. Gonsalves, H.-S. Mao, K. Nakamura, C. Benedetti, C. Schroeder, C. Tóth, J. Daniels, D. Mittelberger, S. Bulanov *et al. Phys. Rev. Lett*., **113**:245002, 2014.

[24] W. Lu, M. Tzoufras, C. Joshi, F. S. Tsung, W. B. Mori, J. Vieira, R. A. Fonseca, and L. O. Silva. *Phys. Rev. ST Accel. Beams*, **10**:061301, 2007.

[25] P. Sprangle, Cha-Mei Tang, and E. Esarey. *Plasma Science, IEEE Transactions on*, **15**:145, 1987.